Journal of Organometallic Chemistry 897 (2019) 207–216

Contents lists available at ScienceDirect

Journal of Organometallic Chemistry

journal homepage: www.elsevier.com/locate/jorganchem

Synthesis, biological evaluation and colorimetric sensing studies of platinum group metal complexes comprising pyrazine based thiourea derivatives

Lathewdeipor Shadap [a], Siewdorlang Diamai [a], Jaya Lakshmi Tyagi [b], Krishna Mohan Poluri [b], Werner Kaminsky [c], Mohan Rao Kollipara [a, *]

[a] Centre for Advanced Studies in Chemistry, North-Eastern Hill University, Shillong, 793 022, India
[b] Department of Biotechnology and Centre for Nanotechnology, Indian Institute of Technology Roorkee, Roorkee, 247 667, India
[c] Department of Chemistry, University of Washington, Seattle, WA, 98195, USA

ARTICLE INFO

Article history:
Received 11 June 2019
Received in revised form
6 July 2019
Accepted 8 July 2019
Available online 11 July 2019

Keywords:
Ruthenium
Rhodium
Iridium
Thiourea derivatives

ABSTRACT

A series of complexes (**1**–**9**) were synthesized by the reaction of halide bridged metal precursors with the three pyrazine thiourea ligands **L1**, **L2** and **L3** to yield cationic as well as neutral complexes and characterized by various spectroscopic techniques. The cationic complexes are represented by the general formula $[(arene)M(L)Cl]^+$, where **L** = **L1**, **L2** and **L3**, arene = *p*-cymene, Cp* and M = Ru, Rh and Ir. All the cationic complexes were isolated with chloride/PF_6 as the counter ion. Reactions of rhodium and iridium dimers with **L2** yielded neutral complexes **5** and **6** with the general formula $[(arene)M(L)Cl_2]$. The neutral complexes **5** and **6** were further reacted with NaN_3 to yield azido complexes **10** and **11**. These complexes were, in turn, reacted with acetylene derivatives to yield triazolo complexes **12**–**15** where only a few triazolo complexes of Cp* have been reported. X-ray diffraction studies revealed the complexes having a typical piano stool geometry around the metal center with the thiourea adducts binding to the metal center in a chelating (N, S) manner. Furthermore, the complexes **1**–**9,** as well as the ligands were screened for potential anti-bacterial agents out of which complexes **3** and **5** exhibited anti-bacterial activity. Colorimetric sensing studies showed the agglomeration of the silver NPs upon addition of the ligands while the complexes were unresponsive.

1. Introduction

Either bactericidal or bacteriostatic is the strategy of anti-bacterial agents and many a time, an eventual growth arrest or cell death may lead to increased drug resistance [1]. Hence, new anti-bacterial designs and regimes are needed to combat such concerns. From the reported literature, thiourea derivatives have proven to be quite biologically active (as anti-cancer agents, anti-microbial, anti-fungal, *etc.*) which has been the subject of investigation by various research groups [2–7]. Thiourea derivatives have been noted for their versatile coordination to metal centers as neutral, monobasic or dibasic ligands and their complexes have revealed importance as anti-cancer, anti-bacterial, anti-fungal agents [8]. On the other hand, half-sandwich complexes of some platinum group metals (such as Ru, Rh, Ir, Os) especially dimeric chloro-bridged complexes have proven to be very significant in the field of organometallic chemistry owing to fact that they bear unique properties such as, to readily form stable complexes with various ligands, their mild reaction conditions for synthesis, high yields *etc.*, which paved way for their usefulness as starting precursors [9,10]. Nonetheless, the nature of the arene ring, the chelating ligand as well as the leaving group in some way or the other can influence the chemical and biological activity and can even sway structural activity (modes of binding) of various complexes where in the case of half sandwich complexes, the chloride can be substituted with azide (N_3) group which may lead to a strained coordination [11] which can be further carried out towards the formation of triazolo complexes. Due to increased drug-resistant and side effects, our quest is to find new and alternative drugs that can minimize such disquiets and one of the ways that can be done is through drug modification. The burgeoning design of arene metal precursors are the amphiphilic nature of the arene

* Corresponding author.
E-mail address: mohanrao59@gmail.com (M.R. Kollipara).

https://doi.org/10.1016/j.jorganchem.2019.07.011
0022-328X/

metal unit, provided by the hydrophobic arene ligand counter balanced by the hydrophilic metal center, and the synthetic diversity of the arene ligand, which is an excellent scaffold for the coupling of ligand-metal complexes for targeted chemotherapy [12]. The biological importance of both thiourea derivatives and metal precursors has prompted us to explore the biological applications of arene complexes containing thiourea ligands. Apart from biological importance, these thiourea derivatives have been reported to show response towards colorimetric sensing activity using silver Nano-particles, which gives good agglomeration effects due to the sulfur atom [13]. Gold and silver nanoparticles based sensing have received much attention to various analytical areas such as chemical sensing and bio-sensing, as well as in medicine due to their immense potential for cancer diagnosing and therapy since their sizes are similar to the biological molecules and structures and such studies, have been explored for the detection of various analytes such as alkali and alkaline earth metal ions, heavy metal ions, anions, biological assay such proteins, oligonucleotides and some organic molecules [14].

In this study, we concoct the thiourea by employing 2-amino pyrazine with benzoyl isothiocyanate, phenyl isothiocyanate and benzyl isothiocyanate yielding **L1**, **L2** and **L3** (Chart 1). These ligands were prepared according to the reported procedures [15] with modification by replacing the amino-substituent by 2-amino pyrazine. We herein report the synthesis, characterization and anti-bacterial screening of arene metal complexes containing pyrazine based thiourea derivatives as well as colorimetric sensing study of thiourea derivative ligands for sensitive identification and detection.

2. Experimental

2.1. Materials and methods

α-phellandrene, pentamethylcyclopentadiene were purchased from Sigma Aldrich and all the reagents purchased were of good commercial quality and used without further purification. Benzoyl isothiocyanate, phenyl isothiocyanate, benzyl isothiocyanate and 2-aminopyrazine were obtained from Spectrochem, Alfa Aesar and S. D. Fine Chem. Pvt. Ltd. The drying and distilling of the solvents were done in accordance with the standard procedures [16]. Starting metal precursor [(*p*-cymene)Ru(μ-Cl)Cl]$_2$ was prepared according to the published procedure [17] and [Cp*MCl$_2$]$_2$ (M = Rh/Ir) were prepared using a synthesizer, Anton par mono-wave 50, where, in a 10 ml sample tube, 500 mg of Rh/IrCl$_3$.nH$_2$O was taken in 2 ml of methanol and 0.4 ml of Cp* was added. The reaction was carried out for 45 min with a temperature set at 110 °C and pressure set at 20 bar. On completion, the reaction was cooled down to a temperature of 60 °C. A maroon crystalline solid and a bright orange powder was obtained for rhodium and iridium precursors respectively. The solid was decanted, washed a few times with diethyl ether, dried and collected. The rhodium and iridium precursors were of a good yield. The synthesized complexes were characterized by FT-IR, ^{1}H NMR, Mass, UV–Vis, and single-crystal X-ray diffraction techniques where Infrared spectra (KBr pellets; 400-4000 cm^{-1}) were recorded on a PerkinElmer 983 spectrophotometer. ^{1}H NMR spectra were recorded on a Bruker Advance II 400 MHz spectrometer using CDCl$_3$/DMSO-d_6 as solvent; chemical shifts were referenced to TMS. Mass spectra were recorded with Q-Tof APCI-MS instrument (model HAB 273) and micrOTOF-Q II 10337 using acetonitrile as solvent. Absorption spectra were recorded on a PerkinElmer Lambda 25 UV–Vis spectrophotometer in the range of 200–600 nm in acetonitrile at room temperature.

2.2. Structure determination by X-ray crystallography

To understand the bonding modes of the complexes, suitable crystals were selected for crystallographic studies. The single crystal data for the complexes were collected with Oxford Diffraction Xcalibur Eos Gemini diffractometer using graphite monochromatic Mo-Kα radiation (λ = 0.71073 Å) and a Nonius Kappa CCD FR590 single crystal X-ray diffractometer, Mo-radiation. The scheme for the data collection was evaluated using the CrysAlisPro CCD software. Crystal data were collected by standard "phi–omega scan" techniques and were scaled and reduced using CrysAlisPro RED software and for complex **11**, the data was integrated and scaled using hkl-SCALEPACK. The structure solution was carried out by SHELXT and refined by full-matrix least squares method based on F^2 against all reflections using SHELXL-2016 [18]. All metal atoms were located from the E-maps and all non-hydrogen atoms were refined anisotropically by full-matrix least-squares. Hydrogen atoms were placed in geometrically idealized positions and constrained to ride on their parent atoms with C–H distances in the range 0.95–1.00 A. Isotropic thermal parameters U$_{eq}$ were fixed such that they were 1.2 U$_{eq}$ of their parent atom Ueq for CH's and 1.5 U$_{eq}$ of their parent atom U$_{eq}$ in case of methyl groups. Table 1 gives the crystallographic and structure refinement parameters for the complexes and selected bond lengths and bond angles are presented in Table 2. The molecular structures were drawn using ORTEP-3 [19], packing pattern and interactions like π-π, H-bonding can be obtained using MERCURY [20].

2.3. Antibacterial activity

All strains were tested for purity by standard microbiological methods. An agar-well diffusion method [20] was employed for evaluation of the compounds for antibacterial activities. Each well diffusion experiment was performed in triplicate with 1 mg ml^{-1} concentration of complexes. Dimethylsulphoxide (DMSO) was used as a solvent and as a negative control, whereas kanamycin antibiotic was used as positive control.

2.4. Colorimetric sensing for ligands and complexes using silver nanoparticles

2.4.1. Synthesis of glutathione capped silver nanoparticles

In a conical flask, 100 ml of 10^{-4} M AgNO$_3$ solution was taken and stirred for a few minutes. 0.01 g of NaBH$_4$ was added to this solution under mild stirring. Yellow colloidal silver nanoparticles was obtained at this step and 200 μL of 0.1 M NaOH was added to maintain the pH of the solution at 10. 100 μL of 10^{-2} M glutathione was added to the yellow colloidal silver NPs to stabilize it. Before studies, the solution was kept overnight and to characterize the synthesized silver nanoparticles, UV–Visible spectrophotometer and Transmission Electron Microscopy (TEM) were used as reported in our previous study [13].

2.4.2. Colorimetric study

To the silver nanoparticles solution, the calculated concentration of the compounds dissolved in DMSO was added and kept for 2–3 h for which only a slight decrease in the intensity was observed using UV–Visible spectrophotometer. The compound solutions were then kept standing overnight for a pronounced effect to be observed and the colorimetric study was conducted using UV–Visible spectrophotometer.

2.5. General procedure for synthesis of metal complexes (1–9)

Metal precursors [(arene)MCl$_2$]$_2$ and thiourea pyrazine

Table 1
Crystal structure data and refinement of complexes **2**, **4**, **6** and **11**.

Complexes	[2]	[4] Cl	[6] Cl	[11]
Empirical formula	$C_{23}H_{26}Cl_5N_4ORhS$	$C_{21}H_{26}Cl_2N_4ORuS$	$C_{21}H_{24}ClIrN_4S$	$C_{21}H_{24}IrN_7S$
Formula weight	686.70	554.49	592.15	598.73
Temperature (K)	296(2)	291(2)	293.10(11)	295(2)
Wavelength (Å)	0.71073	0.71073	0.71073	0.71073
Crystal system	monoclinic	Triclinic	Monoclinic	Triclinic
Space group	*P 21/n*	*P* $\bar{1}$	*P* $2_1/c$	*P* $\bar{1}$
a (Å)/α (°)	10.9552(6)/90	9.2384(4)/97.793(4)	17.4096(13)/90	8.8607(4)/113.057(3)
b (Å)/β (°)	11.6338(6)/90.814(5)	11.0496(6)/101.933(4)	7.5317(5)/99.606(7)	10.2168(7)/95.922(4)
c (Å)/γ (°)	22.1100(11)/90	11.6016(6)/98.454(4)	16.9993(13)/90	13.0289(10)/95.914(4)
Volume ($Å^3$)	2817.6(3)	1129.13(10)	2197.8(3)	1066.12(12)
Z	4	2	4	2
Density (calc) (Mg/m^{-3})	1.619	1.631	1.79	1.865
Absorption coefficient	1.179	1.044	6.305	6.383
F(000)	1384	564	1152	584
Crystal size (mm^3)	0.23 × 0.21 x 0.12	0.16 × 0.15 x 0.12	0.26 × 0.23 x 0.21	0.50 × 0.24 x 0.21
Theta range for data collection	3.9600–28.4440°	4.171–28.585°	4.09–28.261°	2.340–28.304°
Index ranges	−14 ≤ h<=14, −12 ≤ k<=15, −29 ≤ l<=29	−12 ≤ h<=7, −14 ≤ k<=14, −15 ≤ l<=15	−22 ≤ h<=11, −9 ≤ k<=10, −21 ≤ l < 22	−10 ≤ h<=11, −13 ≤ k<=13, −17 ≤ l<=17
Reflections collected	11458	7466	8536	8709
Independent reflections	6459 [R(int) = 0.0291]	5068 [R(int) = 0.0236]	5007 [R(int) = 0.0344]	5224 [R(int) = 0.0682]
Completeness to theta = 25.00°	99.23%	99.27%	99.18%	99.8%
Absorption correction	Semi-empirical from equivalents	Semi-empirical from equivalents	Semi-empirical from equivalents	Semi-empirical from equivalents
Refinement method	Full-matrix least-squares on F^2	Full-matrix least-squares on F^2	Full-matrix least-squares on F2	Full-matrix least-squares on F2
Data/restraints/ parameters	6459/0/314	5068/3/286	5007/38/256	5224/0/276
Goodness-of-fit on F_2	1.059	1.053	1.121	1.068
Final R indices [I > 2sigma(I)]	R1 = 0.0527, w*R2* = 0.1172	R1 = 0.0393, w*R2* = 0.0801	R1 = 0.0471, w*R2* = 0.0776	R1 = 0.0343, w*R2* = 0.0759
R indices (all data)	R1 = 0.0737, w*R2* = 0.1290	R1 = 0.0505, w*R2* = 0.0865	R1 = 0.0625, w*R2* = 0.0828	R1 = 0.0429, w*R2* = 0.0784
Largest diff. peak and hole (e.$Å^{-3}$)	0.833 and −0.698	0.746 and −0.649	1.834 and −1.891	1.762 and −1.859
CCDC No.	1921708	1921706	1921707	1938662

Structures were refined on F_0^2: $wR_2 = [\Sigma[w(F_0^2 - F_c^2)^2]/\Sigma w(F_0^2)^2]^{1/2}$, where $w^{-1} = [\Sigma(F_0^2)+(aP)^2+bP]$ and $P = [\max(F_0^2, 0) + 2F_c^2]/3$.

Table 2
Selected bond lengths (Å) and bond angles (°) of complexes.

Complexes	2	4	6	11
M(1)-CNT	1.793	1.689	1.801	1.800
M(1)-N(3)	2.099(3)	2.111(2)	2.088(5)	2.085(4)
M(1)-S(1)	2.3517(11)	2.3818(8)	2.3779(16)	2.3690(12)
M(1)-Cl(1)	2.3783(12)	2.4067(9)	2.3953(17)	–
M(1)-N(5)	–	–	–	2.113(4)
N(3)-M(1)-S(1)	87.05(10)	84.38(7)	84.10(15)	83.77(11)
N(3)-M(1)-Cl(1)	88.25(10)	87.38(7)	86.19(15)	–
N(3)-M(1)-N(5)	–	–	–	87.06(16)
N(5)-M(1)-S(1)	–	–	–	89.76(14)
Cl(1)-M(1)-S(1)	88.57(4)	86.55(3)	88.49(6)	–

CNT represents the centroid of the arene/Cp* ring and (M = Ru, Rh and Ir).

derivative ligands (**L1**, **L2** and **L3**) were taken (ratio 1:2) in dry acetone (10 ml) and stirred at room temperature for 4 h to yield metal complexes **1**–**9** (Schemes 1 and 2). The complexes precipitated during the reaction time and the precipitate was centrifuged, decanted, washed with diethyl ether (2 × 5 ml) and air dried. The complexes **7**–**9** were partially soluble in chloroform, dichloromethane and acetonitrile so, complexes **7**–**9** were taken and stirred in methanol for an additional 1 h and NH_4PF_6 was added. After 1 h, the reaction mixture was fully evaporated and dichloromethane was added where the compound was fully soluble leaving NH_4Cl salt and was filtered off through celite. The dichloromethane solution was reduced and hexane was added to precipitate out the compound. Overall, all these complexes are soluble in acetonitrile, chloroform, dichloromethane and are insoluble in non-polar solvents like hexane, pet ether, *etc.*

2.5.1. [(p-cymene)Ru(L1)Cl]Cl (1)

Yield: 0.052 g (76%); dark yellow; FT-IR (KBr, cm^{-1}): 3435 $\nu_{(NH)}$, 1711 $\nu_{(C=O)}$, 1509 $\nu_{(C=N)}$, 1138 $\nu_{(C=S)}$; ^1H NMR (400 MHz, $CDCl_3$, ppm) = 13.69 (s, 1H), 12.24 (s,1H), 8.87 (s, 1H), 8.83 (d, 1H, *J* = 4 Hz),

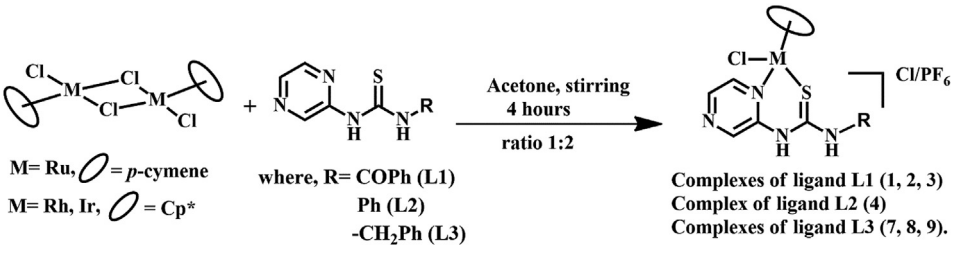

Scheme 1. Synthesis of cationic complexes.

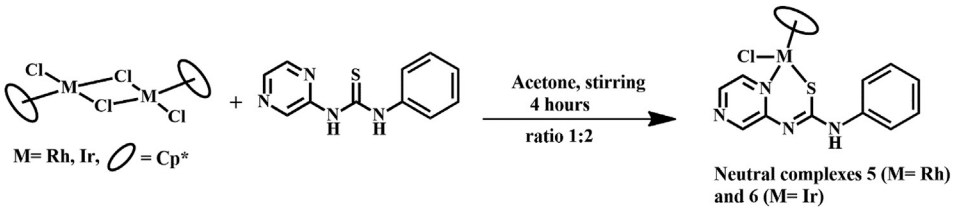

Scheme 2. Synthesis of neutral complexes.

8.43 (d, 1H, $J = 4$ Hz), 7.61 (d, 2H, $J = 8$ Hz) 7.51–7.48 (m, 2H), 7.43–7.40 (m, 1H), 5.63 (d, 1H, $J = 8$ Hz, $CH_{p\text{-cym}}$, 5.54 (d, 1H, $J = 4$ Hz, $CH_{p\text{-cym}}$, 5.47 (d, 2H, $J = 4$ Hz, $CH_{p\text{-cym}}$, 2.61–2.58 (sept, 1H, $CH_{p\text{-cym}}$, 2.06 (s, 3H), 1.28–1.25 (d, 6H, $J = 4$ Hz); ^{13}C NMR (100 MH, $CDCl_3$ + DMSO-d_6, ppm) = 179.41, 168.14, 148.54, 146.30, 141.85, 139.61, 133.93, 130.80, 128.86, 128.33,106.60, 101.52, 87.95, 85.90, 85.00, 84.78, 30.13, 21.93, 21.57, 17.55; Mass- ESI (m/z): calculated: 493.59, found: 495.08 [M-2Cl + H]$^+$; UV–Vis {Acetonitrile, λ_{max}, nm ($\varepsilon/10^{-4}$ M^{-1} cm^{-1})}: 259 (2.844), 311 (1.743), 423 (0.215)).

2.5.2. [Cp*Rh(L1)Cl]Cl (2)

Yield: 0.060 g (82%); orange; FT-IR (KBr, cm^{-1}): 3429 $\nu_{(NH)}$, 1709 $\nu_{(C=O)}$, 1517 $\nu_{(C=N)}$, 1138 $\nu_{(C=S)}$; ^{1}H NMR (400 MHz, $CDCl_3$, ppm) = 8.63 (d, 1H, $J = 4$ Hz), 8.52 (s, 1H), 8.36 (s, 2H), 7.66 (t, 1H, $J = 8$ Hz), 7.58 (t, 3H, $J = 8$ Hz), 1.65 (s, 15H, $CH_{(Cp^*)}$); ^{13}C NMR (100 MH, $CDCl_3$ + DMSO-d_6, ppm) = 173.31, 161.63, 149.23, 147.45, 144.45, 144.33, 134.04, 130.69, 129.49, 128.73,96.23, 95.69, 8.32; Mass- ESI (m/z): calculated: 497.44, found: 495.10 [M-2Cl–2H]$^+$; UV–Vis {Acetonitrile, λ_{max}, nm ($\varepsilon/10^{-4}$ M^{-1} cm^{-1})}: 235 (2.894), 263 (2.376), 410 (0.2485).

2.5.3. [Cp*Ir(L1)Cl]Cl (3)

Yield: 0.054 g (77%); yellow; FT-IR (KBr, cm^{-1}): 3434 $\nu_{(NH)}$, 1709 $\nu_{(C=O)}$, 1518 $\nu_{(C=N)}$, 1138 $\nu_{(C=S)}$; ^{1}H NMR (400 MHz, $CDCl_3$ + DMSO-d_6, ppm) = 8.93 (s, 1H), 8.55 (s, 1H), 8.48–8.43 (m, 1H), 8.28 (d, 1H, $J = 8$ Hz), 7.69–7.63 (m, 1H), 7.62–7.52 (m, 3H), 1.65 (s, 15H, $CH_{(Cp^*)}$); ^{13}C NMR (100 MH, $CDCl_3$ + DMSO-d_6, ppm) = 170.31, 159.46, 148.28, 147.61, 137.72, 136.52, 130.22, 128.97, 128.41,95.82, 8.28; Mass- ESI (m/z): calculated: 586.75, found: 585.17 [M-2Cl–2H]$^+$; UV–Vis {Acetonitrile, λ_{max}, nm ($\varepsilon/10^{-4}$ M^{-1} cm^{-1})}: 261 (3.165), 288 (2.943), 420 (0.392).

2.5.4. [(p-cymene) Ru(L2)Cl]Cl (4)

Yield: 0.065 g (88%); dark yellow; FT-IR (KBr, cm^{-1}): 3441 $\nu_{(NH)}$, 1515 $\nu_{(C=N)}$, 1141 $\nu_{(C=S)}$; ^{1}H NMR (400 MHz, $CDCl_3$, ppm) = 8.93 (s, 1H), 8.33 (s, 1H), 8.78 (s, 1H), 8.40 (s, 1H), 7.62 (d, 2H, $J = 8$ Hz), 7.48 (t, 2H, $J = 8$ Hz), 7.40 (t, 1H, $J = 8$ Hz), 5.56 (s, 1H) $_{pcym}$, 5.49 (s, 1H) $_{pcym}$, 5.35 (s, 2H) $_{pcym}$, 2.89–2.80 (sept, 1H) $_{pcym}$, 2.03 (s, 3H) $_{pcym}$, 1.26 (d, 6H, $J = 8$ Hz) $_{pcym}$; ^{13}C NMR (100 MH, $CDCl_3$ + DMSO-d_6, ppm) = 148.30, 129.40, 125.25, 86.99, 85.93, 85.81, 84.55, 30.67, 30.46, 22.28, 21.91, 18.38, 18.16; Mass- ESI (m/z): calculated: 465.58, found: 465.10 [M-2Cl–H]$^+$; UV–Vis {Acetonitrile, λ_{max}, nm ($\varepsilon/10^{-4}$ M^{-1} cm^{-1})}: 237 (2.713), 315 (1.591).

2.5.5. [Cp*Rh(L2)Cl] (5)

Yield: 0.058 g (79%); orange; FT-IR (KBr, cm^{-1}): 3435 $\nu_{(NH)}$, 1520 $\nu_{(C=N)}$, 1122 $\nu_{(C=S)}$; ^{1}H NMR (400 MHz, $CDCl_3$ ppm) = 10.42 (s, 1H), 8.62 (s, 1H), 8.38 (s, 1H), 8.33 (s, 1H), 8.04 (d, 2H, $J = 8$ Hz), 7.53 (t, 2H, $J = 8$ Hz), 7.26 (t, 1H, $J = 8$ Hz), 1.73 (s, 15H, $CH_{(Cp^*)}$); ^{13}C NMR (100 MH, $CDCl_3$, ppm) = 150.35, 135.85, 128.34, 125.57, 121.51, 95.37, 58.81, 8.55; Mass- ESI (m/z): calculated: 469.43, found: 467.14 [M-2Cl–2H]$^+$; UV–Vis {Acetonitrile, λ_{max}, nm ($\varepsilon/10^{-4}$ M^{-1} cm^{-1}}: 236 (2.805), 269 (2.229), 316 (1.270).

2.5.6. [Cp*Ir(L2)Cl] (6)

Yield:0.062 g (86%); yellow; FT-IR (KBr, cm^{-1}): 3434 $\nu_{(NH)}$, 1517 $\nu_{(C=N)}$, 1124 $\nu_{(C=S)}$; ^{1}H NMR (400 MHz, $CDCl_3$ + DMSO-d_6, ppm) = 8.50 (s, 1H), 8.29 (t, 1H, $J = 12$ Hz), 8.12 (s, 2H), 8.02 (d, 1H, $J = 8$ Hz), 7.62 (d, 1H, $J = 8$ Hz), 7.55 (d, 2H, $J = 4$ Hz), 1.63 (s, 15H, $CH_{(Cp^*)}$); ^{13}C NMR (100 MH, $CDCl_3$ + DMSO-d_6, ppm) = 150.85, 141.33, 138.62, 135.33, 130.11, 125.72, 121.41, 96.45, 96.13, 8.42; Mass- ESI (m/z): calculated: 558.74, found: 557.20 [M-2Cl–2H]$^+$; UV–Vis {Acetonitrile, λ_{max}, nm ($\varepsilon/10^{-4}$ M^{-1} cm^{-1}}: 234 (2.752), 274 (2.079), 317 (1.607).

2.5.7. [(p-cymene) Ru(L3)Cl]PF_6 (7)

Yield: 0.061 g (85%); yellowish-orange; FT-IR (KBr, cm^{-1}): 3432 $\nu_{(NH)}$, 1518 $\nu_{(C=N)}$, 1127 $\nu_{(C=S)}$, 843 $\nu_{(P-F)}$; ^{1}H NMR (400 MHz, $CDCl_3$, ppm) = 11.24 (s, 1H), 8.41 (s, 1H), 7.84 (d, 2H, $J = 8$ Hz), 7.77 (s, 2H), 7.52 (s, 1H), 7.38 (d, 2H, $J = 4$ Hz), 6.90 (d, 2H, $J = 8$ Hz), 5.68 (d,2H, $J = 8$ Hz) $_{pcym}$, 5.62 (d, 2H, $J = 4$ Hz) $_{pcym}$, 3.08–2.97 (sept, 1H) $_{pcym}$, 2.26 (s, 3H) $_{pcym}$, 1.30 (d, 6H, $J = 8$ Hz) $_{pcym}$; ^{13}C NMR (100 MH, $CDCl_3$ + DMSO-d_6, ppm) = 156.94, 155.99, 141.97, 137.59, 135.57, 132.67, 131.39, 106.73, 102.44, 99.84, 96.63, 86.44, 85.33, 82.26, 81.93, 30.10, 29.91, 21.81, 21.44, 17.84, 17.61; Mass- ESI (m/z): calculated: 479.60, found: 479.0815 [M-2Cl–H]$^+$; UV–Vis {Acetonitrile, λ_{max}, nm ($\varepsilon/10^{-4}$ M^{-1} cm^{-1}}: 225 (2.802), 313 (0.975), 415 (0.142).

2.5.8. [Cp*Rh(L3)Cl]PF_6 (8)

Yield: 0.058 g (79%); orange; FT-IR (KBr, cm^{-1}): 3422 $\nu_{(NH)}$, 1522 $\nu_{(C=N)}$, 1116 $\nu_{(C=S)}$, 848 $\nu_{(P-F)}$; ^{1}H NMR (400 MHz, $CDCl_3$ + DMSO-d_6, ppm) = 8.26 (s, 1H), 8.13 (s, 1H), 8.02 (s, 1H), 7.94 (s, 1H), 7.86–7.81 (m, 3H), 7.70 (s, 1H), 6.83 (s, 2H), 1.58 (s, 15H, $CH_{(Cp^*)}$); ^{13}C NMR (100 MH, $CDCl_3$ + DMSO-d_6, ppm) = 153.90, 156.22, 143.30, 142.61, 138.51, 131.37, 130.19, 96.03, 95.89, 8.53; Mass- ESI (m/z): calculated: 483.46, found: 481.0898 [M-2Cl–2H]$^+$; UV–Vis {Acetonitrile, λ_{max}, nm ($\varepsilon/10^{-4}$ M^{-1} cm^{-1}}: 226 (3.998), 313 (1.170), 391 (0.1335).

2.5.9. [Cp*Ir(L3)Cl]PF_6 (9)

Yield: 0.061 g (82%); light yellow; FT-IR (KBr, cm^{-1}): 3447 $\nu_{(NH)}$, 1514 $\nu_{(C=N)}$, 1124 $\nu_{(C=S)}$, 848 $\nu_{(P-F)}$; ^{1}H NMR (400 MHz, $CDCl_3$ + DMSO-d_6, ppm) = 8.70 (s, 1H), 8.21 (s, 1H), 7.91–7.85 (m, 3H), 7.62 (s, 1H), 7.33 (d, 2H, $J = 8$ Hz), 6.79 (d, 2H, $J = 8$ Hz), 1.63 (s, 15H, $CH_{(Cp^*)}$); ^{13}C NMR (100 MH, $CDCl_3$ + DMSO-d_6, ppm) = 157.41, 155.58, 144.87, 141.38, 134.71, 132.44, 131.92, 131.66, 96.45, 95.37, 8.28; Mass- ESI (m/z): calculated: 572.77, found: 571.1806 [M-2Cl–2H]$^+$; UV–Vis {Acetonitrile, λ_{max}, nm ($\varepsilon/10^{-4}$ M^{-1} cm^{-1}}: 228 (3.073), 314 (1.362).

2.6. General procedure for synthesis of metal-azido complexes (10 and 11)

The neutral complexes **5** and **6** were further reacted with NaN_3 in methanol in the ratio of 1:4 (complex: NaN_3), stirred for 8 h at room temperature to yield complexes **10** and **11** (Scheme 3). Upon adding NaN_3, a color change was observed where in the case of complex **5**, the color of the reaction mixture changed from orange

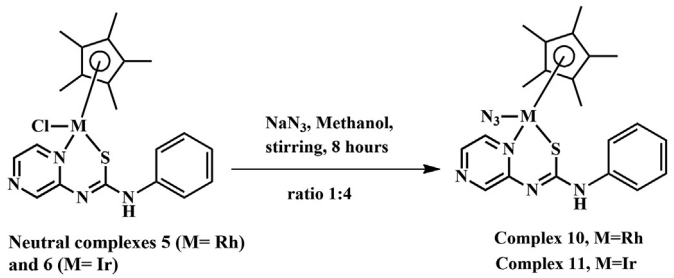

Scheme 3. Synthesis of azido complexes.

to maroon color while in the case of complex **6**, the color changed from light yellow to orange color. Upon the completion of the reaction, the precipitate was centrifuged, washed with diethyl ether and air dried. These complexes were found to be highly soluble in polar solvents like dichloromethane, chloroform, acetonitrile, *etc*, and insoluble in all non-polar solvents and were of good yield. The azido complexes were characterized using various spectroscopic techniques.

*2.6.1. [Cp*Rh(L2)N3] (10)*

Yield: 0.050 g (70%); deep red; FT-IR (KBr, cm^{-1}): 3424 $\nu_{(NH)}$, 2014 $\nu_{(N3)}$, 1548 $\nu_{(C=N)}$, 1132 $\nu_{(C=S)}$; ^{1}H NMR (400 MHz, DMSO-d_6, ppm) = 9.60 (s, 1H), 8.18 (d, 2H, J = 20 Hz), 8.05 (s, 1H), 7.82 (d, 2H, J = 8 Hz), 7.32 (t, 2H, J = 8 Hz), 7.07 (t, 1H, J = 8 Hz), 1.61 (s, 15H, $CH_{(Cp^*)}$); ^{13}C NMR (100 MH, $CDCl_3$ + DMSO-d_6, ppm) = 154.72, 143.59, 143.32, 139.86, 136.94, 128.15, 122.90, 95.45, 95.38, 7.94; Mass- ESI (m/z): calculated: 511.45, found: 468.32 [M-N_3-H]$^+$.

*2.6.2. [Cp*Ir(L2)N3] (11)*

Yield: 0.061 g (82%); orange; FT-IR (KBr, cm^{-1}): 3423 $\nu_{(NH)}$, 2035 $\nu_{(N3)}$, 1595 $\nu_{(C=N)}$, 1153 $\nu_{(C=S)}$; ^{1}H NMR (400 MHz, $CDCl_3$, ppm) = 8.72 (s, 1H), 8.57 (m, 2H), 8.33 (d, 1H, J = 8 Hz), 8.01 (d, 1H, J = 4 Hz), 7.85 (t, 1H, J = 4 Hz), 7.51 (d, 2H, J = 8 Hz), 7.49 (m, 1H), 1.59 (s, 15H, $CH_{(Cp^*)}$); ^{13}C NMR (100 MH, $CDCl_3$, ppm) = 153.26, 144.78, 143.63, 139.84, 137.07, 128.26, 123.07, 121.33, 88.10, 7.78; Mass- ESI (m/z): calculated: 559.15, found: 557.54 [M-N_3-H]$^+$.

2.7. General procedure for synthesis of metal-triazolo complexes (12–15)

The synthesized complexes **10** and **11** were further reacted with acetylene derivatives (DMAD/DEAD) in dichloromethane, stirred for 12 h to yield triazolo complexes (**12**–**15**) (Scheme 4). The azido complexes were completely soluble in dichloromethane and upon adding acetylene derivatives a color change was observed where the color of the solutions of all the triazolo complexes ranged from dark maroon to brown color. At the end of the reaction, the solution was concentrated to 1–2 ml and hexane was added to precipitate the compound. The precipitated compound was washed with

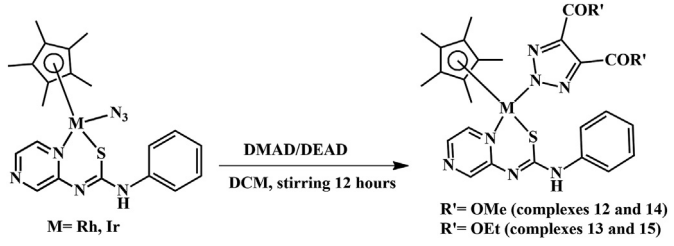

Scheme 4. Synthesis of triazolo complexes.

diethyl ether and dried. All the triazolo complexes were soluble in polar solvents and insoluble in non-polar solvents. These complexes were characterized by various spectroscopic methods.

*2.7.1. [Cp*Rh(L2){N3C2(CO2Me)2}] (12)*

Yield: 0.058 g (78%); yellowish brown; FT-IR (KBr, cm^{-1}): 3421 $\nu_{(NH)}$, 1731 $\nu_{(-CO2-)}$, 1595 $\nu_{(C=N)}$, 1153 $\nu_{(C=S)}$; ^{1}H NMR (400 MHz, $CDCl_3$, ppm) = 8.94 (s, 1H), 8.25 (s, 1H), 8.03 (d, 1H, J = 4 Hz), 7.88 (s, 1H), 7.69 (d, 2H, J = 8 Hz), 7.36 (t, 2H, J = 8 Hz), 7.28 (s, 1H), 7.13 (t, 1H, J = 8 Hz), 3.90 (s, 6H), 1.53 (s, 15H, $CH_{(Cp^*)}$); ^{13}C NMR (100 MH, $CDCl_3$, ppm) = 161.34, 145.32, 144.23, 128.63, 93.71, 54.83, 12.01, 7.84; Mass- ESI (m/z): calculated: 469.09, found: 467.31 [M-triazole-2H]$^+$.

*2.7.2. [Cp*Rh(L2){N3C2(CO2Et)2}] (13)*

Yield: 0.050 g (75%); light brown; FT-IR (KBr, cm^{-1}): 3447 $\nu_{(NH)}$, 1725 $\nu_{(-CO2-)}$, 1595 $\nu_{(C=N)}$, 1160 $\nu_{(C=S)}$; ^{1}H NMR (400 MHz, DMSO-d_6, ppm) = 8.89 (s, 1H), 8.20 (s, 1H), 8.10 (s, 1H), 8.01 (d, 2H, J = 8 Hz), 7.82 (m, 1H), 7.79 (m, 2H), 7.36 (s, 1H), 4.32 (q, 4H, J = 8 Hz), 1.57 (s, 15H, $CH_{(Cp^*)}$), 1.40 (t, 6H, J = 8 Hz); ^{13}C NMR (100 MH, DMSO-d_6, ppm) = 162.30, 155.25, 144.29, 143.52, 140.80, 136.49, 128.33, 96.87, 60.36, 13.83, 8.12; Mass- ESI (m/z): calculated: 681.61, found: 680.05 [M – 2H]$^+$, 467.04 [M-triazole-2H]$^+$.

*2.7.3. [Cp*Ir(L2){N3C2(CO2Me)2}] (14)*

Yield: 0.045 g (70%); brown; FT-IR (KBr, cm^{-1}): 3449 $\nu_{(NH)}$, 1731 $\nu_{(-CO2-)}$, 1513 $\nu_{(C=N)}$, 1158 $\nu_{(C=S)}$; ^{1}H NMR (400 MHz, DMSO-d_6, ppm) = 8.69 (s, 1H), 8.15 (s, 1H), 7.87 (s, 1H), 7.79 (s, 3H), 7.31 (t, 2H, J = 8 Hz), 7.08 (d, 1H, J = 8 Hz), 3.85 (s, 6H), 1.55 (s, 15H, $CH_{(Cp^*)}$); ^{13}C NMR (100 MH, DMSO-d_6, ppm) = 162.05, 144.62, 143.81, 140.29, 128.25, 89.57, 51.44, 11.51, 7.73; Mass- ESI (m/z): calculated: 559.15, found: 557.13 [M-triazole-2H]$^+$.

*2.7.4. [Cp*Ir(L2){N3C2(CO2Et)2}] (15)*

Yield: 0.043 g (68%); light brown; FT-IR (KBr, cm^{-1}): 3424 $\nu_{(NH)}$, 1735 $\nu_{(-CO2-)}$, 1595 $\nu_{(C=N)}$, 1153 $\nu_{(C=S)}$; ^{1}H NMR (400 MHz, DMSO-d_6, ppm) = 8.68 (s, 1H), 8.15 (s, 1H), 8.01 (s, 1H), 7.89 (s, 1H), 7.81 (d, 2H, J = 8 Hz), 7.30 (t, 2H, J = 8 Hz), 7.06 (t, 1H, J = 8 Hz), 4.29 (q, 4H, J = 8 Hz), 1.54 (s, 15H, $CH_{(Cp^*)}$), 1.33 (t, 6H, J = 8 Hz); ^{13}C NMR (100 MH, DMSO-d_6, ppm) = 163.01, 151.71, 143.72, 140.31, 128.33, 93.41, 56.11, 13.72, 7.92; Mass- ESI (m/z): calculated: 559.15, found: 556.75 [M-triazole-2H]$^+$.

3. Results and discussion

3.1. Synthesis of metal complexes

In this study, the metal complexes **1**–**9** were prepared according to the general procedure given in the experimental section. Ruthenium complexes yielded yellowish-brown precipitate whereas rhodium and iridium complexes yielded orange to yellow colored precipitates. Complexes were isolated as cationic as well as neutral complexes. In case of cationic complexes, complexes **1**–**4** have chloride as the counter ion while complexes **7**–**9** have PF_6 as counter ion. In all these complexes, coordination to the metal center takes place in a bidentate N, S chelating fashion. Interestingly, Rh and Ir dimers upon reaction with ligand **L2**, yielded neutral complexes **5** and **6** while with ruthenium dimer yielded a cationic complex. Overall, all these complexes were soluble in polar solvents and insoluble in non-polar solvents like hexane, pet-ether, *etc*. Reactions of NaN_3 with neutral complexes **5** and **6**, yielded azido complexes **10** and **11** respectively. The azido complexes **10**, **11** (Scheme 3) were of good yield and highly soluble in polar solvents. The complexes **10**, **11** were further reacted with acetylene derivatives [21] which yielded triazolo complexes **12**–**15** (Scheme 4).

These triazolo complexes of rhodium and iridium are one of the few complexes reported as compared to the triazolo complexes of ruthenium. All of these complexes were of good yield and air stable.

3.2. Spectral studies of complexes

3.2.1. FT-IR spectroscopy

The presence of functional groups in a compound can help us identify its formation and this can be achieved by IR spectroscopy study. The binding of the ligands through specific groups to the metal center can also be determined to some extent based on the increase as well as decrease of the stretching frequencies. In these synthesized complexes, the N–H stretching frequencies were observed in the range 3308–3434 cm^{-1} for free ligands and around 3421-3449 cm^{-1} for metal complexes which are more or less incomparable and indicated that there is no bonding through N–H nitrogen to the metal center. The stretching frequency of C=O group in ligand **L1** was observed around 1695 cm^{-1} whereas that of complexes **1**–**3** was observed around 1709-1711 cm^{-1} which showed that the C=O bonding is intact and strong which revealed that there was no bonding of the oxygen of carbonyl group to the metal center. The stretching frequency of C=S in free ligands was observed around the range 1159–1169 cm^{-1} whereas in the complexes, it shifted to a lower frequency *i.e.* 1116-1160 cm^{-1} indicating that bonding takes place through sulfur atom to the metal center [22]. In case of the cationic complexes where PF_6 behaved as the counter ion, the stretching frequency of P–F bond was observed at around 843-848 cm^{-1}. In the case of azido complexes **10** and **11**, the presence of the azide group can be confirmed by the signal observed at 2014 cm^{-1} and 2035 cm^{-1} respectively (Figs. S1–S6) while in the case of the triazolo complexes **12**–**15**, the azide signal was absent. In complexes **12** and **14**, the presence of the ester group was observed at 1731 cm^{-1} respectively while for complexes **13** and **15**, the ester group was observed at 1725 cm^{-1} and 1735 cm^{-1} respectively. These IR data showed the formation of the complexes by detecting the most prominent groups present in the complexes and gave us a preview of the composition and coordination of metal complexes.

3.2.2. ^{1}H NMR studies of the complexes

The ^{1}H NMR spectra of the complexes have been provided in the supplementary information (Figs. S7–S15). N–H signals were observed in the aromatic region around 10.42–13.69 ppm as well as in the signal range of the aromatic protons of the ligands but in some complexes, the N–H proton signals were not observed which may be due to solvent interaction. All the ligand protons were observed in the region 6.79–9.60 ppm. We observed that there is an unusual splitting pattern of signal for *p*-cymene moiety (**1**, **4** and **7**) from the usual splitting of the aromatic protons of the *p*-cymene. In complexes **1,** the aromatic proton signals of *p*-cymene split into three doublets at 5.63 ppm, 5.54 ppm and 5.47 ppm, while in complex **4**, was observed two singlets at 5.56 ppm and 5.49 ppm and one doublet at 5.35 ppm. As for complex **7**, two doublets around 5.68 ppm and 5.62 ppm were observed. We also noted two doublets for the six-methyl protons of *p*-cymene instead of one doublet in the range 1.25–1.30 ppm for all the ruthenium *p*-cymene complexes. This unusual pattern is due to the metal is a stereogenic center and, therefore, the aromatic and methyl isopropyl protons of the p-cymene ligand are diastereotopic when coordinated to the thiourea ligands [23]. For complexes **1**, **4** and **7** we observed the septet signal in the range 2.58–3.08 ppm and singlet signal for methyl protons of *p*-cymene were observed around 2.03–2.26 ppm. In rhodium and iridium complexes, in addition to the proton signals of the thiourea ligands, we also observed a sharp singlet around 1.58–1.65 ppm corresponding to Cp* protons. In the case of the azido complexes **10** and **11**, the ^{1}H NMR did not change much but in the case of the triazolo complexes **12**–**15**, well distinct information was obtained wherein the case of complexes **12** and **14**, apart from the aromatic signals of the ligand and the Cp* signal, a sharp signal of the dimethyl group of the acetylene precursor dimethyl acetylene dicarboxylate (DMAD), was observed at 3.90 ppm and 3.85 ppm respectively bearing six protons each while in the case of complexes **13** and **15** containing diethyl acetylene dicarboxylate group, the methylene group was observed as a quartet at 4.32 ppm and 4.29 ppm bearing four protons and for the methyl group, a triplet was observed at 1.40 ppm and 1.33 ppm bearing six protons. On the basis of these NMR data of the triazolo complexes, it is clear that the metal center is bonded to the triazolo group through the central nitrogen which gives a symmetric geometry of the triazole group. Overall, the NMR spectra of all the complexes were of good resonance and integration with the expected formulation of the complexes.

3.2.3. ^{13}C NMR studies of the complexes

The coordination of the ligands to the metal centers is further substantiated by ^{13}C NMR. The spectra of some of the complexes have been given in the supplementary data (Figs. S16–S23). The spectra showed the aromatic carbon signals for the ligands around 117.90–176.56 ppm. In case of complexes **1**–**3**, we observed the C=O signal around 170.31–179.41 ppm while the C=S signal in all the complexes was observed to be in the range 150.35–168 ppm. The carbons of the *p*-cymene rings were observed around 81.93–106.60 ppm while that of the methyl, methine and isopropyl carbons of the *p*-cymene ring were observed around 17.55–30.67 ppm. The methyl carbons of the Cp* ring were observed around 7.73–8.53 ppm and the carbons of the Cp* ring were observed at 88.10–96.87 ppm. Overall, these results support the formation of the complexes.

3.2.4. Mass studies of the complexes

The mass spectra of the complexes have been provided in the supplementary data (Figures. S24- S34) and their values have been given in the experimental section. The found molecular ion peaks (for each complex) were displayed at *m/z*: 495.08 (**1**), *m/z*: 495.10 (**2**), *m/z*: 585.17 (**3**), *m/z*: 465.10 (**4**), *m/z*: 467.14 (**5**), *m/z*: 557.20 (**6**), *m/z*: 479.0815 (**7**), *m/z*: 481.0898 (**8**), *m/z*: 571.1806 (**9**), 468.32(**10**), 557.54 (**11**), 467.31 (**12**), 680.05 and 467.04 (**13**), 557.13 (**14**) and 556.75 (**15**). In addition to the molecular ion peaks, all the complexes except complexes **8** and **10**, isotopic mass peaks were also observed. The molecular ion peaks for the ruthenium complexes **1** corresponded to $[M\text{-}2Cl + H]^{+}$ while complexes **4** and **7** corresponded to $[M\text{-}2Cl\text{–}H]^{+}$. The molecular ion peaks of all the rhodium and iridium complexes corresponded to $[M\text{-}2Cl\text{–}2H]^{+}$. The molecular ion peaks of the azido complexes corresponded to $[M\text{-}N_3\text{-}H]^{+}$ while the triazolo complexes corresponded to [M-triazole-2H]$^{+}$. The consistent and tallied data of the molecular ion peaks of the complexes with the calculated masses shows the formation of the complexes and that there is a strong bonding of the arene rings (arene = *p*-cymene, Cp*) to the metal atom.

3.2.5. UV–Visible description of metal complexes

The electronic spectra of the metal complexes have been provided in the supplementary data (Fig. S35) where they have been recorded in acetonitrile with 10^{-4} M concentrations at room temperature. Since these complexes are d^6 low spin metal complexes, the metal center contains filled d orbitals of proper geometry which can interact with the empty low-lying π^* orbitals of the ligands which may result in metal-to-ligand charge transfer (MLCT) transitions. The low energy absorption band observed in the range 311–423 nm is assigned to the metal-to-ligand charge transfer

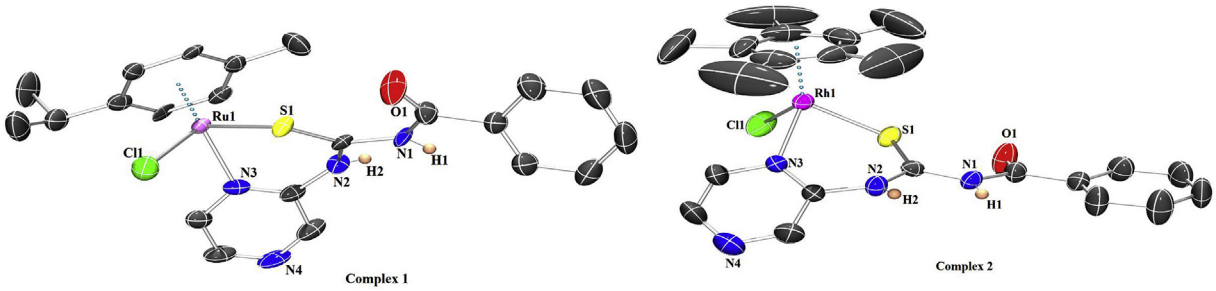

Fig. 1. ORTEP diagram of complexes **1** and **2** where, complex **1** has just been given here to show the composition and mode of binding of the complex. Hydrogen atoms (except NH protons) and counter ions have been omitted for clarity.

(MLCT) dπ(M) to π*(L) transitions while the high energy absorption band observed in the range 225–261 nm may be attributed to ligand-centered π- π*/n- π* transitions.

3.2.6. *Description of molecular structures of metal complexes*

Crystallography study gives us the knowledge of a variety of binding modes and coordination in the metal complexes which other spectroscopic studies are unable to do so. In this structural analysis, we have been able to establish the crystal structures of the represented metal complexes. The ORTEP view of the isolated crystal structures **1**, **2**, **4**, **5**, **6** and **11** with atom numbering are presented in Figs. 1–3 where complexes **2** and **5** due to low theta value, their molecular structures have been given just to show their modes of binding and the relevant crystallographic parameters along with the details of bond lengths; bond angles are listed in Tables 1 and 2 For complexes **1**, **2** and **4**, X-ray studies revealed that these complexes are cationic complexes bearing the general formula $[(arene)M(L)Cl]^{+}$ except complexes **5** and **6** are neutral complexes bearing the general formula [(arene)M(L)Cl]. The molecular structures of the cationic complexes revealed the thiourea derivative ligands bind to the metal in a bidentate manner through nitrogen of the pyrazine ring and thione sulfur donor atoms leading to the formation of a six membered chelated ring.

In complex **5** and **6**, we observed that the binding of the ligand to the metal center showed a typical N, S chelating bonding which resulted in the formation of neutral complexes where the ligand binds to the metal center through the nitrogen of the pyrazine ring and thiol sulfur (SH) upon deprotonation of thiol proton. Through this study, the presence/absence of the N–H proton could be clearly observed where in case of the cationic complexes both the N–H protons were observed while in the case of the neutral complexes one proton was observed while the other was deprotonated (N2) which resulted in the delocalization of the electrons towards the thione sulfur. Complexes **2**, **5** and **6** crystallized in monoclinic system with space group *P 21/n* (for **2** and **5**) and *P* $2_1/c$ (**6**), while complexes **1**, **4** and **11** crystallized in triclinic system with space

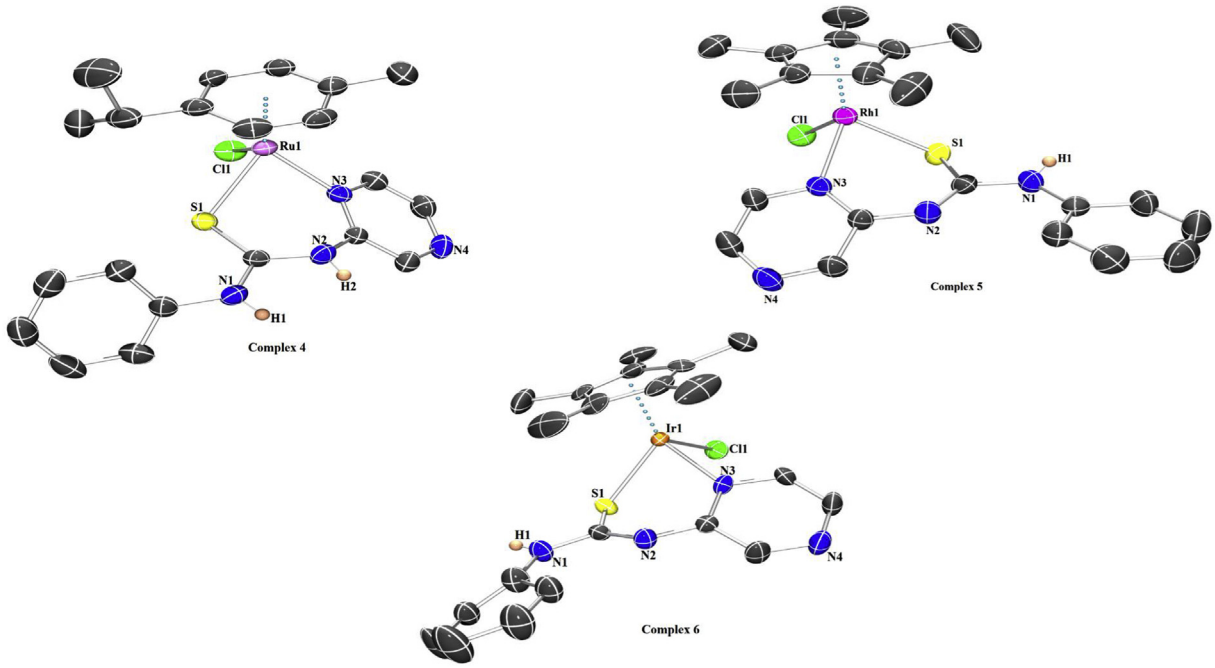

Fig. 2. ORTEP diagram of complexes **4**, **5** and **6** where, complex **5** has just been given here to show the composition and mode of binding of the complex. Hydrogen atoms (except NH protons) and counter ions have been omitted for clarity.

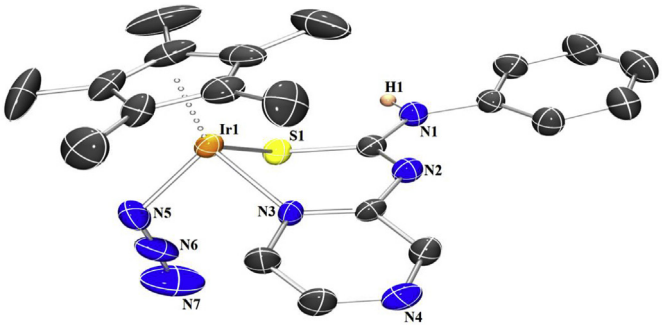

Fig. 3. ORTEP diagram of complexes **11**. Hydrogen atoms (except NH protons) and counter ions have been omitted for clarity.

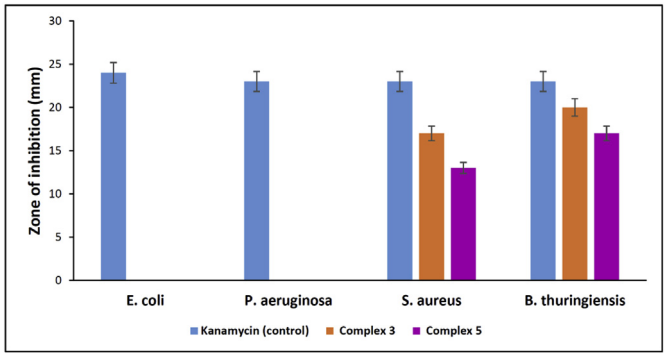

Fig. 4. Antibacterial results of complexes **3** and **5** against Gram-positive (*S. aureus* and *B. thuringiensis*) bacteria with kanamycin as the reference.

group $P\,\bar{1}$ respectively. The distance between the metal (M) to centroid of the arene/Cp* ring, metal to nitrogen M(1)-N(3), metal to sulfur M(1)-S(1) and metal to chloride M(1)-Cl(1) as well as the respective bond angles were given in Table 2. The M – Cl bond lengths in these complexes were found to be comparable to the previously reported values [24,25]. The C=S bond distances of the cationic complexes **1**, **2** and **4** were found to be 1.648(6) Å, 1.676(4) Å, 1.701(3) Å respectively which are in good agreement with the previous reported compounds for C=S [26] whereas in complexes **5** and **6** the C–S bond distance was found to be 1.742(3) Å and 1.754(7) Å respectively which corresponded to C–S single bond. This shows that there is proton delocalization and that metal binds to sulfur as thiol sulfur.

Inter-Hydrogen bonding in the represented complexes was observed where the cationic complexes showed an interaction between N–H protons and the counter ion (Cl^-) while the neutral complexes showed an interaction between the non-bonded pyrazine nitrogen and the N–H proton [Figs. S36–S38]. In complexes **1**, **2** and **4**, H(1)––Cl(2) distances were found to be 2.317 Å, 2.366 Å and 2.449 Å respectively and H(2)––Cl(2) distances were found to be 2.372 Å, 2.250 Å and 2.320 Å respectively while for the neutral complexes **5**, **6** and **11** the N(4)––H(1) distances were found to be 2.369 Å, 2.268 Å and 2.459 Å respectively.

3.2.7. In-vitro antibacterial assay

The ligands and all the synthesized complexes were evaluated for antibacterial study using zone inhibition assay to exert their *in-vitro* antibacterial activity against gram-positive Bacterium *S. aureus* and *B. thuringiensis* and gram-negative bacteria *E. coli* and *P. aeruginosa*. The zones of inhibition (mm) in comparison to kanamycin which was used as a positive control are given in (Fig. 4, Fig. S39 and Table S1). Not all of the compounds exhibited antibacterial activity against the tested organisms where the *in-vitro* assay results revealed only complex **3** and complex **5** showed good activity against gram-positive (*S. aureus* and *B. thuringiensis*) only. Towards *S. aureus*, complexes **3** and **5** showed activity 17 ± 1 mm and 13 ± 1 mm respectively and towards *B. thuringiensis* complexes **3** and **5** showed activity 20 ± 2 mm and 17 ± 1. The active complexes were tested for longer incubation periods *i.e,* even after 72 h, no bacterial colonies were grown in the presence of these complexes, thus confirming that these complexes are bactericidal. All of the ligands showed no activity towards gram-positive nor gram-negative bacteria.

3.2.8. Colorimetric sensing studies

Thiourea derivative ligands have been reported to show colorimetric sensing in room temperature due to the presence of free

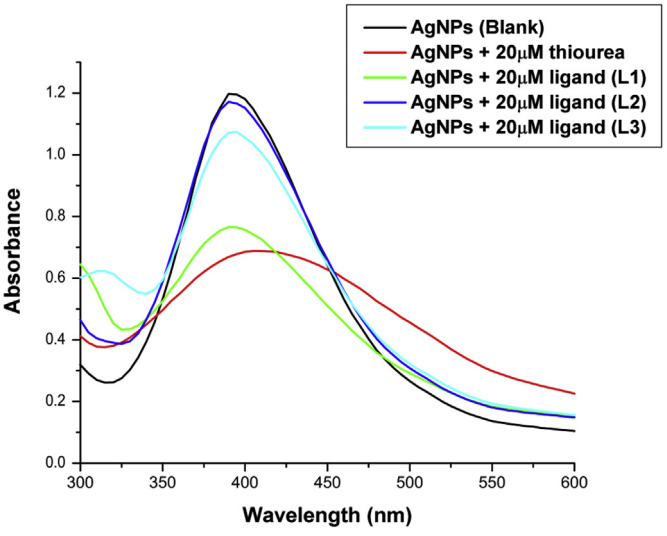

Fig. 5. SPR (Surface Plasmon Resonance) band of ligands **L1**, **L2**, **L3** and thiourea as the reference.

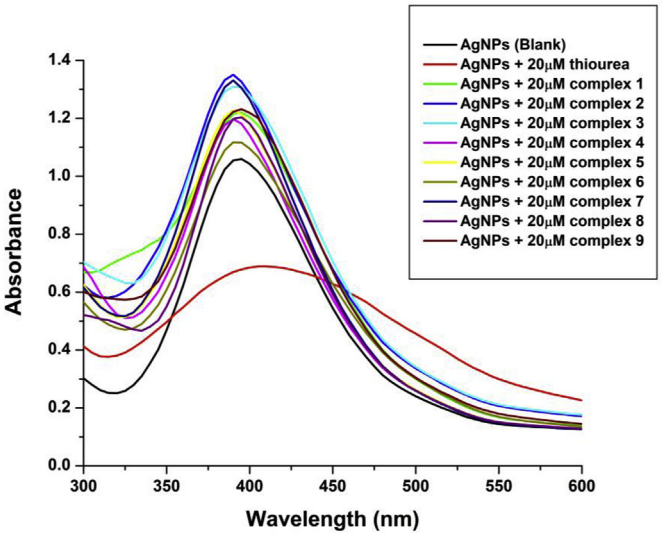

Fig. 6. SPR band of complexes and thiourea as the reference.

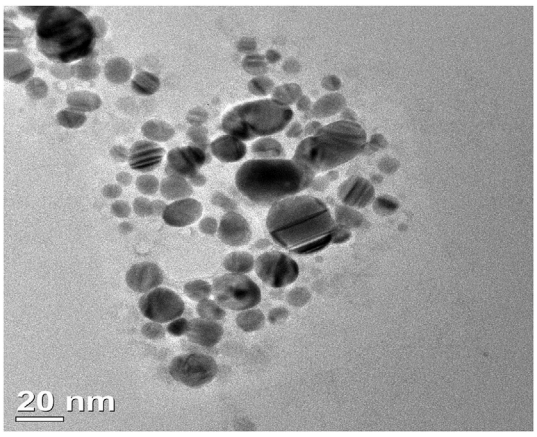

Fig. 7. TEM image of the silver NPs due to ligand **L1**.

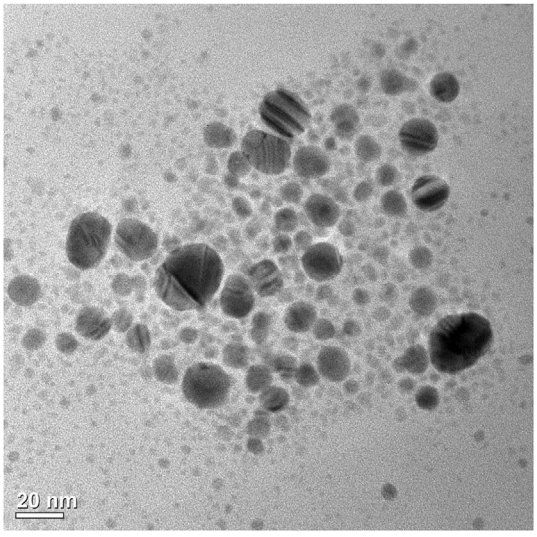

Fig. 8. TEM image of the silver NPs due to ligand **L3**.

sulfur atom [13]. Colorimetric sensing was carried out for all the complexes as well as the ligands. We had taken glutathione capped silver nanoparticles for the study and thiourea as the reference to the various thiourea derivatives. 20 μM of each ligand, complexes and thiourea were added to 5 ml of the silver NPs solution and kept the solutions overnight. The solutions were recorded by UV–Vis spectrophotometer where the SPR (Surface Plasmon Resonance) band of the thiourea and ligands dropped in the intensity (Fig. 5) which suggested that agglomeration had taken place. Amongst the ligands, **L1** showed the most agglomeration effect followed by ligand **L3** and was accompanied with color change (Fig. S40) while ligand **L2** showed the least effect which could also be supported through the distinctive decrease in intensity of the SPR band. In the case of complexes, no color change was observed (Fig. S41) and an increase in intensity was observed with respect to the intensity of the silver NPs (blank) (Fig. 6) rather than a decrease in the intensity which could be attributed to the fact that in the case of the complexes, the silver NPs are hindered from aggregating with each other. The presence of free sulfur in the ligands resulted in agglomeration of the silver NPs where the free sulfur binds to the surface of the silver NPs and causes subsequent agglomeration [27,28], but in case of the complexes, no change was observed in the intensity band because the sulfur is bonded to the metal center, thereby agglomeration is hindered. Upon addition of the ligands to the silver NPs, TEM images revealed the agglomeration of the NPs which are presented in Figs. 7 and 8. TEM images indicate that ligand **L1** can cause agglomeration of the AgNPs more effectively than ligand **L3**. This can be seen from the increased in particles size and shape upon addition of ligand **L1** in which maximum NPs sizes are almost in the ranges ~30 nm, while on the other hand addition of ligand **L3** has a small effect on the aggregation of the NPs, with maximum particles sizes below 20 nm.

4. Conclusion

In summary, we have successfully synthesized ruthenium, rhodium and iridium complexes containing pyrazine thiourea ligands. These complexes were characterized by various spectroscopic techniques and the molecular structures of some of the complexes have been isolated by single crystal XRD which revealed the molecular composition as well as coordination of the ligands towards the metal center. The thiourea ligands bind to the metal center in a bidentate N, S fashion forming cationic complexes with chloride or PF_6 as the counter ion except in complexes **5** and **6**, we observed the formation of N, S neutral complexes. These neutral complexes were reacted further with NaN_3 to yield azido complexes (**10** and **11**) and acetylene derivatives to yield complexes **12**–**15**. The antibacterial activity of the complexes, as well as, the ligands were evaluated against gram-positive (*S. aureus* and *B. thuringiensis*) and gram-negative (*E. coli* and *P. aeruginosa*) bacteria with Kanamycin as the reference where only complexes **3** and **5** showed antibacterial activity towards the gram-positive bacteria. Besides antibacterial activity studies, colorimetric sensing with thiourea as the reference revealed that the ligands (except **L2**) showed effective agglomeration effects of silver NPs as compared to the metal complexes.

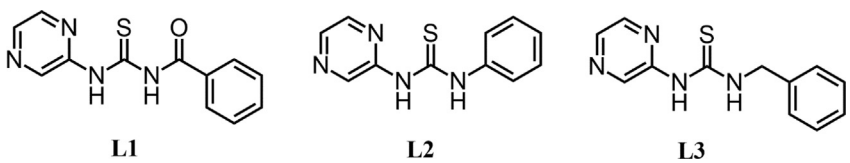

Chart 1. Ligands used in this study.

Acknowledgments

Lathewdeipor Shadap thanks Dr. Basava Punna Rao with his contribution and help, CSIR-NET, New Delhi, India for providing financial assistance in the form of JRF, DST-PURSE SCXRD, NEHU-SAIF, Shillong, India for providing Single Crystal X-ray analysis and other spectral studies.

Appendix A. Supplementary data

Supplementary data to this article can be found online at https://doi.org/10.1016/j.jorganchem.2019.07.011.

References

[1] M.T. Gabr, N.S. El-Gohary, E.R. El-Bendary, M.M. El-Kerdawy, N. Ni, M.I. Shaaban, Chin. Chem. Lett. 26 (2015) 1522–1528.
[2] Y.F. Yuan, J.T. Wang, M.C. Gimeno, A. Laguna, P.G. Jones, Inorg. Chim. Acta 324 (2001) 309.
[3] Y.M. Zhang, T.B. Wei, L. Xian, L.M. Gao, Phosphorus, sulphur, silicon relat, Elements 179 (2004) 2007.
[4] Y.M. Zhang, T.B. Wei, X.C. Wang, S.Y. Yang, Indian J. Chem., Sect. B 37 (1998) 604.
[5] W.Q. Zhou, B.L. Li, L.M. Zhu, J.G. Ding, Z. Yong, L. Lu, X.J. Yang, J. Mol. Struct. 690 (2004) 145.
[6] M. Eweis, S.S. Elkholy, M.Z. Elsabee, Int. J. Biol. Macromol. 38 (2006) 1.
[7] S. Saeed, M.H. Bhatti, M.K. Tahir, P.G. Jones, Acta Crystallogr. E 64 (2008) 1369.
[8] N. Gunasekaran, P. Ramesh, M.N.G. Ponnuswamy, R. Karvembu, Dalton Trans. 40 (2011) 12519.
[9] B. Cornils, W.A. Herrmann, M. Beller, R. Paciello, Applied Homogeneous Catalysis with Organo Metallic Compounds, third ed., VCH, Weinheim, 2018.
[10] P. Govindaswamy, Y.A. Mozharivskyj, M.R. Kollipara, Polyhedron 26 (2007) 5039.
[11] (a) T. Ikariya, S. Kuwata, Y. Kayaki, Pure Appl. Chem. 82 (2010) 1471;
(b) I.L. Mawnai, S. Adhikari, W. Kaminsky, M.R. Kollipara, J. Organomet. Chem. 869 (2018) 26.
[12] P.J. Dyson, Chimia 61 (2007) 698.
[13] (a) L. Shadap, S. Diamai, V. Banothu, D.P.S. Negi, U. Adepally, W. Kaminsky, M.R. Kollipara, J. Organomet. Chem. 884 (2019) 44;
(b) X. Chen, Y. Zhou, X. Peng, J. Yoon, Chem. Soc. Rev. 39 (2010) 1861.
[14] (a) D. Vilela, M.C. González, A. Escarpa, Anal. Chim. Acta 751 (2012) 24;
(b) K. Saha, S.S. Agasti, C. Kim, X. Li, V.M. Rotello, Chem. Rev. 112 (2012) 2739;
(c) O. Elisabete, N. Cristina, S.H. Miguel, F. Javier, F. Adrian, C.J. Luis, L. Carlos, Sens. Actuators B Chem. 212 (2015) 297;
(d) S. Zeng, D. Baillargeat, H.P. Ho, K.Y. Yong, Chem. Soc. Rev. 43 (2014) 3426.
[15] (a) U. Yunus, MdK. Tahir, M.H. Bhatti, S. Alib, W.Y. Wong, Acta Crystallogr. E64 (2008) 20;
(b) K.M. Heda, J. Appl. Chem. 4 (5) (2015) 1541.
[16] D.D. Perrin, W.L.F. Armarego, Purification of Laboratory Chemicals, fourth ed., Butterworths Heinemann, London, 1996.
[17] (a) M.A. Bennett, T.N. Huang, T.W. Matheson, A.K. Smith, S. Ittel, W. Nickerson, Inorg. Synth. 21 (1982) 74.
[18] (a) G.M. Sheldrick, Acta Crystallogr. Sect. A 64 (2008) 112;
(b) G.M. Sheldrick, Acta Crystallogr. C 71 (2015) 3.
[19] L.J. Farrugia, J. Appl. Crystalographica. Sect. C Struct. Chem. 71 (2015) 3–8.
[20] I.J. Bruno, J.C. Cole, P.R. Edgington, M. Kessler, C.F. Macrae, P. McCabe, J. Pearson, R. Taylor, Acta Crystallogr. B 58 (2002) 389–397.
[21] T.A. Albright, R. Hoffmann, J.C. Thibeault, D.L. Thorn, J. Am. Chem. Soc. 101 (1979) 3801.
[22] G. Binzet, N. Kulcu, U. Florke, H. Arslan, J. Coord. Chem. 62 (2009) 3454.
[23] K.T. Prasad, B. Therrien, M.R. Kollipara, J. Organomet. Chem. 693 (2008) 3049.
[24] K. Jeyalakshmi, J. Haribabu, C. Balachandran, N.S.P. Bhuvanesh, N. Emi, R. Karvembu, New J. Chem. 41 (2017) 2672.
[25] M.M. Heeba, M.M. Tamizh, L.J. Farrugia, A. Endo, R. Karvembu, Organomet 33 (2014) 540.
[26] P. Bharati, A. Bharti, M.K. Bharty, B. Maiti, R.J. Butcher, N.K. Singh, Polyhedron 63 (2013) 156.
[27] (a) S. Diamai, W. Warjri, A. Saha, D.P.S. Negi, Colloids Surf., A 538 (2018) 593.
[28] S. Diamai, D.P.S. Negi, Spectrochim. Acta A. 215 (2019) 203.